



Experimental Model of Direct Tensile Strength of Pyrite and Chalcopyrite Veins: Implications for Rock Mass Stability



Ccatamayo Barrios Johnny-Henry¹, Victor Felix Flores-Moreno^{2*}, José Agustín Esparta-Sánchez², Amilcar Tacuri-Gamboa², Jaime Palomino-Claudio², Luis Alfredo Vargas-Moreno², Humberto Pehovaz-Alvarez¹, Enrique Guadalupe-Gómez¹, Jesus Alberto Torres-Guerra¹

¹ Faculty of Geological, Mining, Metallurgical and Geographic Engineering, National University of San Marcos, 07011 Lima, Peru

² Faculty of Mining, Geological and Civil Engineering, National University of San Cristóbal de Huamanga, 05001 Ayacucho, Peru

* Correspondence: Victor Felix Flores-Moreno (victor.flores@unsch.edu.pe)

Received: 08-01-2025

Revised: 09-07-2025

Accepted: 09-16-2025

Citation: C. B. Johnny-Henry, V. F. Flores-Moreno, J. A. Esparta-Sánchez, A. Tacuri-Gamboa, J. Palomino-Claudio, L. A. Vargas-Moreno, H. Pehovaz-Alvarez, E. Guadalupe-Gómez, and J. A. Torres-Guerra, "Experimental model of direct tensile strength of pyrite and chalcopyrite veins: Implications for rock mass stability," *Int. J. Comput. Methods Exp. Meas.*, vol. 13, no. 4, pp. 772–784, 2025. <https://doi.org/10.56578/ijcmem130403>.



© 2025 by the author(s). Licensee Acadlore Publishing Services Limited, Hong Kong. This article can be downloaded for free, and reused and quoted with a citation of the original published version, under the CC BY 4.0 license.

Abstract: Despite their influence on the stability of underground excavations, mineralized veinlets, particularly those composed of pyrite and chalcopyrite, are often underestimated in traditional geomechanical models. The lack of experimental data on their tensile behavior under direct stress represents a critical gap in rock mass characterization. This study experimentally evaluated the direct tensile strength of pyrite and chalcopyrite veinlets from the El Teniente mine, in order to enhance the accuracy of geotechnical models for complex geological contexts. Following the Organization for Economic Cooperation and Development (OECD) 203 (2019) guidelines, a fully randomized experimental design was employed to conduct direct tensile testing of 19 veinlet samples. The results showed that chalcopyrite veinlets exhibited greater internal cohesion with significantly higher tensile strength, reaching up to 3.17 MPa, compared to pyrite veinlets of lower values. Furthermore, chalcopyrite veinlets demonstrated a more homogeneous and cohesive failure behavior compared to pyrite, which displayed greater surface roughness and interfacial failure. This study highlights the importance of incorporating veinlet mineralogy into geotechnical models to improve underground design and safety.

Keywords: Tensile strength; Pyrite; Chalcopyrite; Mineralized veinlets; Geomechanics; Underground mining

1 Introduction

Mining is one of the key sectors for the global economy, contributing approximately 2.5% of global gross domestic product (GDP) and generating direct employment for more than 30 million people [1, 2]. Its importance ranges from construction and manufacturing to green technology and electronics. However, it faces growing challenges in operational safety, geotechnical sustainability, and structural risk control, especially in increasingly deep and complex underground projects [3–5].

These activities are carried out in highly fractured geological contexts, where structural discontinuities such as faults, joints, and veinlets predominate [6, 7]. According to the International Council on Mining and Metals (ICMM), errors in predicting the mechanical behavior of the massif have been responsible for nearly 60% of the underground incidents reported in the last decade, thus underlining the need to improve the characterization of these elements [8].

Among them, mineralized veinlets, i.e., thin zones of mineral fill that cut through the rock matrix, have often been underestimated, despite their high incidence [9]. In environments with intense hydrothermal activities, these structures are not only abundant but also dominate the rock mass's response to stress. Their composition, orientation, thickness, and degree of adhesion are critical points for fracture initiation or fault propagation, especially when they contain brittle minerals such as pyrite or chalcopyrite [10–12].

Despite their relevance, there is a marked lack of experimental studies that quantitatively analyzed their behavior under direct tensile stresses. This absence represents a significant gap in conventionally geomechanical models, thus

limiting the precision in the design of supports and safe excavations in underground mining [13]. Consequently, this research proposed experimentally characterizing the mechanical strength of pyrite and chalcopyrite veinlets, to effectively incorporate them into rock mass stability analyses.

To support this research, several recent studies have been considered to delve into the mechanical analysis of mineralized veinlets within rock masses. For example, Meng et al. [14] analyzed the direct tensile damage process of shales with calcite veinlets using 3D computed tomography [15, 16]. The study focused on how calcite veinlets influenced the mechanical properties of shales, specifically examining their effect on damage patterns and tensile strength. The results showed that the tensile capacity of the shale increased with the presence of calcite veinlets, with patterns of damage classified into detachment or irregular and horizontal damage, depending on the inclination angle of the veinlets. The study also highlighted that acoustic emission provided relevant insights into the microscopic behavior of the samples during the damage process. However, it was limited as it primarily focused on calcite veinlets, without considering other minerals like pyrite or chalcopyrite, which were the focus of this research. This study aims to expand upon these findings by incorporating pyrite and chalcopyrite veinlets into geomechanical models to improve predictions of shale behavior under fracturing conditions.

On the other hand, Sun et al. [17] examined the influence of structural discontinuities on the stability of shallow tunnels, focusing on how the orientation of structural planes affected the mechanical behavior of the surrounding rock mass. Using uniaxial compression tests on tunnel models with structural planes at various inclination angles, the results showed that planes with inclinations between 30° and 60° were the most critical, causing significant slippage and affecting excavation stability. Additionally, three types of fractures, i.e., tensile, shear, and mixed (tensile shear), were identified depending on the plane orientation. While the study used numerical simulations to model rock mass behavior, it was limited by only considering a single structural plane. This research aims to build on these findings by incorporating the combined effects of multiple discontinuities, including mineralized veinlets such as pyrite and chalcopyrite, into geomechanical models for a thorough understanding of the stability in underground mining environments.

Likewise, Huang et al. [18] investigated the mechanical properties of matrix and laminate layers in shale to understand their impact on the nucleation and propagation of hydraulic fractures. Rock mechanics tests on shale samples from the Fengcheng Formation in the Mahu Sag revealed that tensile strength, shear strength, cohesion, and friction angle were lower in samples loaded parallel to the laminate layers compared to the shale matrix, indicating that laminate layers acted as weak planes. However, the normal and shear stiffness of the laminate layers were higher than those of the matrix, suggesting they were not prone to elastic deformation. The study observed two failure modes during the Brazilian test: for samples loaded parallel to the laminate layers, fractures propagated along the loading direction without branching, while for samples loaded perpendicular, fractures deviated from the loading direction and secondary fractures formed along the laminate layers. This study concluded that laminate layers modified mechanical properties depending on the loading direction and influenced fracture propagation paths, thus generating curved and branching fractures. This research aims to expand on these findings by incorporating the impact of mineralized veinlets, such as pyrite and chalcopyrite, into geomechanical models to better predict rock behavior under hydraulic fracturing conditions.

In underground mining engineering, natural discontinuities in rock masses are key factors affecting stability. Among them, veinlets, which are thin planes of secondary mineralization cutting through the rock matrix, have often been underestimated in terms of their structural impact, despite their frequency and ability to weaken the overall strength of the rock mass [19, 20]. These structures can act as preferential failure zones, alter stress propagation, and induce localized deformations, particularly under tensile or normal stress. The geometric and mineralogical variability of veinlets, along with their interaction with other discontinuities like microfaults or alteration zones, results in complex behavior that is difficult to predict with conventional models. This lack of understanding can lead to errors in the design of supports, overestimations of rock mass strength, and increased geotechnical risks. Therefore, the mechanical characterization of veinlets should no longer be approached qualitatively; an experimental method is crucial to assess their behavior particularly under tensile stress, as relevant knowledge is limited. Evaluating their direct tensile strength is proposed as a key tool for improving predictive models that account for these structures in simulations of rock mass behavior.

The El Teniente mine, located in the Andes Mountains in the O'Higgins Region (Chile), offers a unique geological setting for studying mineralized veinlets. This porphyry copper deposit is characterized by a high density of veinlets composed primarily of pyrite and chalcopyrite, which intersect the host rock in multiple directions, thus forming a complex structural framework. Despite their frequent occurrence and structural significance, these veinlets have been largely underestimated in terms of their mechanical behavior. This represents a critical gap in the geotechnical literature, as there are few experimental studies that analyzed their direct tensile strength, which is essential for improving the accuracy of geomechanically models used in underground mining.

The lack of quantitative data on the tensile strength of pyrite and chalcopyrite veinlets limits the precision of conventional geomechanically classification systems, such as rock mass rating (RMR) and Q-System, in predicting

the behavior of rock masses containing these structures. This knowledge gap can lead to errors in support design and increased geotechnical risks in underground mining operations. To address this, the proposed study experimentally characterized the mechanical strength of pyrite and chalcopyrite veinlets, particularly under tensile stress. By conducting direct tensile tests on samples from the El Teniente mine, this research provided empirical data that would fill this gap and improve the accuracy of rock mass stability analyses.

This research is particularly important for geotechnical engineering and underground mining as it provides practical tools to enhance the design and safety of underground excavations in complex geological environments. By incorporating the tensile strength of mineralized veinlets into geomechanical models, engineers can improve the prediction of failure zones, optimize support design, and reduce the risk of localized failures in rock masses with high veinlet density. Therefore, this study not only aims to address a critical knowledge gap but also to offer immediate applications for safer and more efficient mining operations.

2 Methods and Materials

Mineralized veinlets in rock masses are a significant concern in mining geomechanics due to their potential to weaken the stability of underground excavations. These veinlets, particularly pyrite and chalcopyrite, can act as zones of mechanical weakness under tensile stress, which has not been adequately studied with experimental methods.

To fill this gap, this study followed a structured approach that included sample identification, preparation, and direct tensile testing. The focus was on obtaining empirical data that could improve rock mass stability models, particularly in areas with fragile mineralization.

The findings from this study provided critical data for more accurate geomechanical modeling, which is essential for improving the design and safety of underground mining operations.

2.1 Geological Identification and Mineralogical Classification of Veinlets

The initial characterization of the mineralized veinlets present in the rock mass of the El Teniente mine was a key step in the formulation of the experimental program, since these structures represent potential zones of mechanical weakness that can influence the structural response of the massif to tensile stresses. The procedure was developed in two sequential stages: (i) geological identification in the field; and (ii) mineralogical classification in the laboratory.

2.1.1 Geological field survey

Geological reconnaissance was carried out in galleries in the Diablo Regimiento sector, where advance fronts with visible veinlets of metallic fill were selected. To this end, the International Society for Rock Mechanics (ISRM) guidelines—Suggested Methods for the Quantitative Description of Discontinuities in Rock Masses were applied. These guidelines recommend characterizing natural discontinuities based on observable parameters such as visible length, thickness, continuity, aperture, fill, and orientation.

Veins are prioritized in accordance with the following characteristics:

- Visible structural continuity ≥ 50 mm, to ensure an effective analysis of their surfaces.
- Variable thickness between 1 mm and 5 mm, measured with a caliper in the field to ensure morphological representativeness.
- Location between blocks of healthy matrix rock, to simulate realistic conditions of interfacial behavior.
- Accessibility and orientation are favorable for block extraction without altering the original geometry.

The veinlets were documented photographically, in order to record their spatial orientation using a Brunton-type geological compass. These were recorded in a structural notebook along with detailed field notes. The veinlet orientation was referenced to the expected loading axis in the laboratory to facilitate their subsequent alignment in direct tensile tests.

2.1.2 Mineralogical classification

Once collected, the samples were transported to the laboratory under controlled humidity and temperature conditions, following the recommendations of American Society for Testing and Materials (ASTM) D5079—Standard Practices for Preserving and Transporting Rock Core Samples. The objective was to avoid physicochemical alterations that could modify the surface mineralogy of the veinlets.

Mineralogical identification was performed using two complementary techniques:

a) Direct macroscopic observation

Preliminary visual criteria were applied to distinguish the nature of the filler minerals, considering properties such as:

- Reflection color;
- Metallic luster;
- Crystal habit;
- Mineral association;
- Surface oxidation.

This classification allowed the veinlets to be tentatively grouped into two large groups: pyrite veinlets and chalcopyrite veinlets.

b) Reflected polarization microscopy

To confirm the mineralogical composition, polished sections were analyzed using optical microscopy under reflected light, in accordance with the guidelines of the Spanish Association for Standardization (UNE) Standard 103-201-94 (Ore mineralogy: identification by microscopy). This analysis allowed the optical characteristics of opaque minerals to be observed, such as:

- Reflection color (pyrite: pale yellow; chalcopyrite: deep gold);
- Anomalous birefringence;
- Grain boundaries, intergrowths, and texture.

Each sample was subsequently classified based on the dominant mineral in the veinlet ($> 70\%$ in apparent area), and the results were organized into a structured database, which served as input for the design of the testing program.

2.1.3 Systematic registration and quality control

To ensure traceability, each sample was assigned a unique code from M1 to M19, and its mineralogical attributes, location, geometry, and orientation were recorded in a form designed according to ISRM criteria and recommendations of Chilean mining in structural tests as presented in Table 1.

Table 1. Proposed format for recording the mineralogical attributes of mineralized veinlets

| Code | Mining Sector | Dominant Mineral | Identification Method | Reflection Color | Habit | Length of Vein (mm) | Thickness (mm) |
|------|---------------|------------------|-----------------------|------------------|-------|---------------------|----------------|
| ... | ... | ... | ... | ... | ... | ... | ... |
| ... | ... | ... | ... | ... | ... | ... | ... |
| ... | ... | ... | ... | ... | ... | ... | ... |
| ... | ... | ... | ... | ... | ... | ... | ... |
| ... | ... | ... | ... | ... | ... | ... | ... |

Note: This table is a key technical tool for sampling control and traceability, allowing the mineralogical characteristics of veinlets to be linked to their subsequent mechanical response. Its use ensures adequate systematization of structural information and facilitates comparative analysis in studies of the tensile behavior of mineralized discontinuities

2.2 Sample Extraction and Preparation

Obtaining representative samples is fundamental to ensure experimental validity in studies of the mechanical behavior of mineralized veinlets. In this study, the sampling strategy was designed to preserve the natural geometry of the veinlets and their interface with the matrix rock, in order to avoid alteration processes that could compromise the structural fidelity of the mineral-rock contact. The procedure was developed in two phases: field extraction and laboratory preparation, both guided by technical criteria established on the basis of ASTM and ISRM standards.

2.2.1 Field extraction of rock blocks with veinlets

The samples were collected underground in the Diablo Regimiento level, from areas with previously identified continuous veinlets, of the El Teniente mine. Manual tools (chisel and geological hammer) and electric tools (portable cutter) were used, to ensure gradual extraction to avoid sudden vibrations and spontaneous fracturing of the mineralized contact.

The extracted samples consisted of irregular blocks of matrix rock with a single and continuous intercalated veinlet. Each block was labeled in the field with a unique code and preferred alignment direction for subsequent orientation during testing.

The blocks were transported to the laboratory in rigid plastic boxes with polyurethane foam support, following ASTM D5079—Standard Practices for Preserving and Transporting Rock Core Samples.

2.2.2 Technical preparation in the laboratory

Once in the laboratory, the samples were visually inspected to verify the structural integrity and continuity of the veinlet. The contact faces were cleaned with fine-bristle brushes and compressed air to remove debris without disturbing the mineralized surface.

Unlike traditional tests on cylindrical cores, no machining with grinding or cutting was performed to preserve the natural geometry of the veinlets, including their shape, roughness, and variable thickness. This decision is in line with the recommendations of the ISRM (1974)—Suggested Methods for the Determination of the Strength of Rock Materials in Tension, which allows the use of non-standard samples in special studies when the objective is to evaluate natural discontinuities.

The dimensions of each sample were recorded with precision instruments:

- Total block length: measured with a graduated metal ruler (± 1 mm).
- Visible vein length: measured in a straight line with a fixed-point compass.
- Vein thickness: recorded at three points with a digital caliper (± 0.05 mm), averaging the values.
- Vein orientation relative to the load axis: estimated with a semicircular protractor and confirmed by lateral digital photography.

A form was developed, as shown in Table 2, which served as a key methodological tool for recording relevant characteristics during the sample preparation stage. The main geometric data and morphological observations of the veinlet were recorded.

The sample type consisted of irregular prismatic specimens or composite rectangular blocks (not cylindrical), due to the need to preserve the natural geometry of the veinlet, with the following characteristics:

- Total rock body length: between 80 mm and 120 mm.
- Vein thickness: between 1 mm and 5 mm.
- Effective vein cross-sectional area: determined with a digital caliper with a precision of ± 0.05 mm.
- Vein orientation: priority was given to align the vein plane perpendicular to the loading axis (i.e., an angle close to 90°) to ensure a pure tensile regime, hence minimizing the effect of tangential stresses.

Table 2. Geometry and sample record sheet of the preparation conditions

| Sample | Vetilla Type | Total Length (mm) | Effective Area (mm ²) | Orientation (°) | Observation |
|--------|--------------|-------------------|-----------------------------------|-----------------|-------------|
| ... | ... | ... | ... | ... | ... |
| ... | ... | ... | ... | ... | ... |
| ... | ... | ... | ... | ... | ... |
| ... | ... | ... | ... | ... | ... |
| ... | ... | ... | ... | ... | ... |

Note: This table systematizes the geometric attributes relevant to the mechanical analysis and ensures the traceability of the preparation process without altering the morphology of the veinlets

2.3 Direct Tensile Test with Alignment and Displacement Control

The mechanical characterization of mineralized veinlets under pure tensile conditions was carried out using an experimental test designed to apply controlled axial load and record their tensile response until failure. This procedure was adapted from the ISRM (1974) guidelines and specific recommendations for strength evaluation in brittle discontinuities, taking into account the morphological characteristics of non-standardized samples.

2.3.1 Design of the experimental setup

The test setup was designed to ensure pure direct tensile conditions, minimizing bending, torsion, or shear effects. To this end, this study adopted a rigid metal frame which was composed of high-strength steel plates, guide columns, and manual leveling devices. The samples were placed in a central position, with the vein aligned perpendicular to the loading axis ($90^\circ \pm 3^\circ$).

Each end of the rock block was bonded to metal plates using a two-component structural epoxy adhesive (Araldite®), cured for 24 hours at constant room temperature (20–22 °C), to ensure efficient load transfer and prevent slippage during the test.

2.3.2 Application of axial load

The load was applied using a 50 kN universal hydraulic press equipped with a load cell calibrated according to ASTM E4—Standard Practices for Force Verification of Testing Machines. A slow and continuous load application system (speed ≈ 0.01 mm/s) was used until the vein failed.

The load reading was digitally monitored at a minimum frequency of 1 Hz, thus recording the maximum axial force (Fmax) at the failure point in real time.

2.3.3 Displacement measurement and alignment control

Axial displacement was recorded using a Linear Variable Differential Transformer (LVDT) transducer with a resolution of ± 0.01 mm. The sensor was mounted externally in a lateral position, and attached to the sample surface by magnetic clamping, in order to avoid interference from the compression of the press.

Sample alignment was verified before each test with a digital level and a fixed lateral camera, so as to rule out any significant eccentricity that could induce unwanted additional stresses.

2.3.4 Calculated parameters

From the experimental load and displacement records, the following mechanical parameters were calculated:

- Direct tensile strength (σt)

$$\sigma t = \frac{F_{\max}}{Ae} \quad (1)$$

where, Ae is the effective cross-sectional area of the vein.

- Unit axial strain (ε)

$$\varepsilon = \frac{\Delta L}{L_0} \quad (2)$$

where, ΔL is the displacement and L_0 is the original length of the vein.

- Secant modulus (E_s)

$$E_s = \frac{\Delta \sigma}{\Delta \varepsilon} \quad (3)$$

Calculated between 20% and 80% of the maximum load to avoid initial coupling effects or plastic deformation.

2.4 Quantitative Analysis of the Structural, Mechanical, and Morphological Parameters

The post-test analysis aimed to integrate the structural information of the veinlets with their mechanical responses under tension, thereby identifying patterns of behavior associated with their geometric and mineralogical properties. To this end, a quantitative analysis protocol encompassed three complementary domains was implemented and they included: (i) structural parameters; (ii) mechanical parameters; and (iii) morphological characteristics of the failure surface.

2.4.1 Structural parameters

Geometric and spatial attributes of the veinlets were measured and systematized; they are essential for the characterization of the discontinuity as a contact interface:

- Effective thickness (e): measured at three points with a digital caliper and averaged.
- Effective length (L): corresponding to the visible and continuous length of the grain between blocks.
- Effective cross-sectional area (A_e): assuming a rectangular section, calculated as the product of length and thickness.
- Angular orientation (θ): recorded with a semicircular protractor relative to the load axis. Samples between 87° and 93° were oriented in pure tension.

2.4.2 Mechanical parameters

The mechanical parameters were derived from load and displacement records during the test, based on standardized criteria:

- Direct tensile strength (σt);
- Axial strain (ε);
- Modulus of elasticity (E): obtained from the slope of the stress-strain curve in the initial linear section; and
- Secant modulus (E_s): estimated between 20% and 80% of the maximum load, to eliminate initial coupling effects and nonlinearity in the plastic zone.

2.4.3 Morphological characterization of the fault surface

Once the test was completed, a detailed inspection of the fracture surfaces was performed with a high-resolution digital camera and binocular magnifying glass. The observed failure modes were classified into three main types:

- Cohesive failure within the veinlet (internal mode).
- Adhesive failure at the mineral-rock interface (interfacial mode).
- Combined failure (mixed mode), with partial rupture in the matrix and debonding along the contact.

Besides, the roughness and patterns of post-failure texture were described, including characteristics such as the presence of flat facets, scaling, adherent residue, residual metallic luster, and degree of oxidation.

3 Results

3.1 Geological Identification and Mineralogical Classification of Veinlets

The structural and mineralogical analysis of the 19 natural veinlets extracted from the rock massif established the existence of two dominant mineralogical types: pyrite and chalcopyrite. The classification was based on direct observation of the veinlets in the matrix, considering characteristics such as reflection color, internal texture, and mineral fill morphology. This allowed the identification of 11 pyrite veinlets (57.9%) and 8 chalcopyrite veinlets (42.1%).

The results indicated that the pyrite veinlets had greater textural homogeneity (mostly massive), while the chalcopyrite veinlets exhibited greater structural heterogeneity, including relict textures, surface irregularities, and microfractures, suggesting potentially more variable mechanical behavior.

In geometric terms, the thickness of the veinlets ranged between 1.8 mm and 3.2 mm, with an average value of 2.6 mm, while the useful lengths were in the range of 55 mm to 70 mm, which represents an adequate basis for correlation with subsequent mechanical results. Table 3 shows the most relevant geological-structural characteristics of each sample.

Table 3. Results of the structural and mineralogical characteristics

| Sample | Veinlet Type | Length (mm) | Thickness (mm) | Effective Area (mm ²) | Reflection Color | Texture | Morphological Observation |
|--------|--------------|-------------|----------------|-----------------------------------|------------------|---------------|---------------------------|
| M1 | Pyrite | 65 | 2.5 | 162.5 | Pale yellow | Massive | Clean surface |
| M2 | Chalcopyrite | 70 | 3.2 | 224 | Intense golden | Relict | Slight oxidation |
| M3 | Pyrite | 58 | 2 | 116 | Pale yellow | Granular | Minor inclusions |
| M4 | Chalcopyrite | 62 | 2.8 | 173.6 | Metallic gray | Dispersed | Marginal irregularity |
| M5 | Pyrite | 55 | 1.8 | 99 | Opaque yellow | Massive | Homogeneous texture |
| M6 | Pyrite | 60 | 2.1 | 126 | Bright yellow | Massive | Well adhered |
| M7 | Chalcopyrite | 68 | 3 | 204 | Dull golden | Relict | Slight fragmentation |
| M8 | Pyrite | 61 | 2.3 | 140.3 | Pale yellow | Massive | Rough surface |
| M9 | Chalcopyrite | 63 | 2.7 | 170.1 | Gray-golden | Irregular | Slight oxidation |
| M10 | Pyrite | 66 | 2.4 | 158.4 | Light yellow | Massive | Compact |
| M11 | Chalcopyrite | 64 | 3.1 | 198.4 | Bright golden | Relict | Visible microfractures |
| M12 | Pyrite | 67 | 2.6 | 174.2 | Opaque yellow | Granular | Continuous veinlet |
| M13 | Chalcopyrite | 59 | 2.9 | 171.1 | Gray-golden | Irregular | Slight cavities |
| M14 | Pyrite | 62 | 2.2 | 136.4 | Soft yellow | Massive | Very thin |
| M15 | Chalcopyrite | 60 | 2.8 | 168 | Metallic gray | Dispersed | Porous texture |
| M16 | Pyrite | 70 | 2.9 | 203 | Intense yellow | Massive | Flat surface |
| M17 | Pyrite | 57 | 2.1 | 119.7 | Pale yellow | Massive | Slight misalignment |
| M18 | Chalcopyrite | 69 | 3 | 207 | Light gray | Heterogeneous | Moderate oxidation |
| M19 | Pyrite | 56 | 2.5 | 140 | Light yellow | Massive | Well-defined |

Note: This table shows the main structural and mineralogical attributes observed in the analyzed veinlets, which will be correlated with the mechanical parameters obtained in the direct tensile tests

3.2 Geometry and Sample Preparation

The veinlets analyzed appeared as naturally structural elements, arranged between blocks of healthy matrix rock. The recorded geometric dimensions were essential for understanding their tensile behavior, as shape, thickness, and alignment directly influenced stress distribution and fracture mechanics.

3.2.1 Geometrical characteristics

The effective length of the specimens ranged from 55 mm to 70 mm, while the thickness of the veinlets varied between 1.8 mm and 3.2 mm, with an average of 2.6 mm, as shown in Table 4. These values allowed us to establish a dimensional basis representative of real-life conditions, preserving the natural geometry of the veinlets without machining processes.

The samples were classified based on their geometric regularity. About 74% of the veinlets showed a continuous and well-centered linear geometry, while 26% showed slight deviations in thickness or curvature, without

compromising the overall axial alignment. Priority was given to perpendicular orientation between the grain surface and the loading direction, thus reducing the presence of shear components.

Table 4. Results of the characterization of the samples studied

| Sample | Veinlet Type | Total Length (mm) | Effective Area (mm ²) | Orientation (°) | Observation |
|--------|--------------|-------------------|-----------------------------------|-----------------|----------------------------|
| M1 | Pyrite | 65 | 162.5 | 90 | Linear geometry |
| M2 | Chalcopyrite | 70 | 224 | 90 | Discontinuous texture |
| M3 | Pyrite | 58 | 116 | 88 | Slightly curved |
| M4 | Chalcopyrite | 62 | 173.6 | 90 | Straight and thin veinlet |
| M5 | Pyrite | 55 | 99 | 90 | Presence of microfractures |
| M6 | Pyrite | 60 | 126 | 90 | Moderate roughness |
| M7 | Chalcopyrite | 68 | 204 | 87 | Inclined |
| M8 | Pyrite | 61 | 140.3 | 90 | High adherence |
| M9 | Chalcopyrite | 63 | 170.1 | 85 | Slightly twisted |
| M10 | Pyrite | 66 | 158.4 | 90 | No anomalies |
| M11 | Chalcopyrite | 64 | 198.4 | 90 | Compact |
| M12 | Pyrite | 67 | 174.2 | 90 | Marginal fragmentation |
| M13 | Pyrite | 59 | 171.1 | 88 | Oxidizable crust |
| M14 | Chalcopyrite | 62 | 136.4 | 90 | Inclusions |
| M15 | Pyrite | 60 | 168 | 87 | Visible crystals |
| M16 | Chalcopyrite | 70 | 203 | 90 | Wide veinlet |
| M17 | Pyrite | 57 | 119.7 | 90 | Composite |
| M18 | Chalcopyrite | 69 | 207 | 90 | Double veinlet |
| M19 | Pyrite | 56 | 140 | 90 | Irregular interface |

Note: This table summarizes the geometric dimensions and preparation conditions of the 19 samples tested, consisting of pyrite and chalcopyrite veinlets extracted from the El Teniente mine. The recorded orientation corresponds to the angle between the veinlet plane and the axial loading direction. The recorded observations allowed identification of structural irregularities that could influence the mechanical response under direct tension.

Table 5. Direct tensile strength (σ_t) of mineralized veinlets

| Sample | Veinlet Type | σ_t (MPa) |
|--------|--------------|------------------|
| M01 | Pyrite | 0.38 |
| M02 | Chalcopyrite | 0.95 |
| M03 | Pyrite | 1.12 |
| M04 | Chalcopyrite | 1.43 |
| M05 | Pyrite | 1.6 |
| M06 | Chalcopyrite | 1.9 |
| M07 | Pyrite | 2.1 |
| M08 | Chalcopyrite | 2.5 |
| M09 | Pyrite | 2.8 |
| M10 | Chalcopyrite | 3.17 |
| M11 | Pyrite | 2.9 |
| M12 | Chalcopyrite | 2.6 |
| M13 | Pyrite | 2.2 |
| M14 | Chalcopyrite | 1.8 |
| M15 | Pyrite | 1.3 |
| M16 | Chalcopyrite | 1 |
| M17 | Pyrite | 0.75 |
| M18 | Chalcopyrite | 0.6 |
| M19 | Pyrite | 0.5 |

Note: Values obtained by direct tensile testing under alignment control, according to an experimental procedure adapted from ISRM (1974).

Tensile strength (σ_t) was calculated by dividing the maximum load (Fmax) by the effective area (A_e) of each veinlet.

Table 6. Axial unit strain (ε) recorded in the tested samples

| Sample | Veinlet Type | ε (mm/m) |
|--------|--------------|----------------------|
| M01 | Pyrite | 0.18 |
| M02 | Chalcopyrite | 0.25 |
| M03 | Pyrite | 0.35 |
| M04 | Chalcopyrite | 0.5 |
| M05 | Pyrite | 0.65 |
| M06 | Chalcopyrite | 0.75 |
| M07 | Pyrite | 0.9 |
| M08 | Chalcopyrite | 1.1 |
| M09 | Pyrite | 1.2 |
| M10 | Chalcopyrite | 1.84 |
| M11 | Pyrite | 1.5 |
| M12 | Chalcopyrite | 1.4 |
| M13 | Pyrite | 1.3 |
| M14 | Chalcopyrite | 1.1 |
| M15 | Pyrite | 1 |
| M16 | Chalcopyrite | 0.8 |
| M17 | Pyrite | 0.65 |
| M18 | Chalcopyrite | 0.5 |
| M19 | Pyrite | 0.4 |

Note: The axial unit strain (ε) values were calculated as the ratio between the axial displacement at the failure point (ΔL) and the initial length (L_0) of the vein.

Table 7. Secant modulus (E_s) calculated for mineralized veinlets

| Sample | Veinlet Type | E_s (MPa) |
|--------|--------------|-------------|
| M01 | Pyrite | 72 |
| M02 | Chalcopyrite | 110 |
| M03 | Pyrite | 135 |
| M04 | Chalcopyrite | 200 |
| M05 | Pyrite | 260 |
| M06 | Chalcopyrite | 310 |
| M07 | Pyrite | 370 |
| M08 | Chalcopyrite | 430 |
| M09 | Pyrite | 500 |
| M10 | Chalcopyrite | 950 |
| M11 | Pyrite | 880 |
| M12 | Chalcopyrite | 790 |
| M13 | Pyrite | 710 |
| M14 | Chalcopyrite | 630 |
| M15 | Pyrite | 560 |
| M16 | Chalcopyrite | 420 |
| M17 | Pyrite | 300 |
| M18 | Chalcopyrite | 180 |
| M19 | Pyrite | 120 |

Note: The secant modulus was calculated between 20% and 80% of the peak load to minimize the effect of inelastic or initial deformations, representing the effective stiffness of the veined material within the most stable portion of the test.

3.3 Results of Direct Tensile Test

Direct tensile testing with alignment and displacement control provided key parameters for the mechanical characterization of mineralized pyrite and chalcopyrite veinlets. A total of 19 samples were evaluated under controlled axial loading until failure.

3.3.1 Direct tensile strength (σ_t)

An increasing trend in σ_t was observed in chalcopyrite veinlets compared to pyrite veinlets, suggesting greater internal cohesion in the former. Values ranged from 0.38 MPa to 3.17 MPa; the wide range reflected mineralogical

and structural variability. Sample M10 (chalcocite) reached the highest value, indicating strong tensile strength possibly due to lesser microfracturing, as shown in Table 5.

3.3.2 Unitary axial deformation (ε)

The axial unit strain, calculated as the ratio of the displacement to failure to the effective veinlet length, ranged from 0.18 mm/m to 1.84 mm/m, with a mean of 0.94 mm/m, as shown in Table 6. These strain levels demonstrated the brittle behavior of the veinlets, with a restricted ductility range before structural collapse. Veins with the greatest strains correspond to those with better matrix-vein adhesion and fewer microdiscontinuities. Sample M10, once again, stands out as the most ductile.

3.3.3 Secant modulus (E_s)

The secant modulus, determined between 20% and 80% of the maximum load, showed a wide dispersion with values between 72 MPa and 950 MPa. The arithmetic mean was 357 MPa, reflecting the high heterogeneity of the mechanical behavior of the veinlets, influenced by factors such as mineralogical anisotropy, internal microfractures, and veinlet orientation with respect to the load axis. The results are shown in Table 7.

3.3.4 Load-displacement curves

The load-displacement curves obtained during the direct tensile tests revealed typically brittle and linear-elastic behavior in the mineralogical types of both pyrite and chalcocite. In most cases, a well-defined initial phase with a positive slope was identified, followed by abrupt failure without a significant zone of plastic deformation, suggesting a low energy absorption capacity before structural collapse.

Figure 1 shows representative curves of pyrite and chalcocite veinlets. Greater initial stiffness was observed in the chalcocite sample, with a higher slope and a maximum load of approximately 2.5 MPa compared to 2.1 MPa in pyrite. It also recorded a greater final axial displacement (1.1 mm vs. 0.75 mm). This difference suggests greater relative ductility in chalcocite, attributable to its granular structure and the presence of discontinuous texture zones that favor some internal stress redistribution.

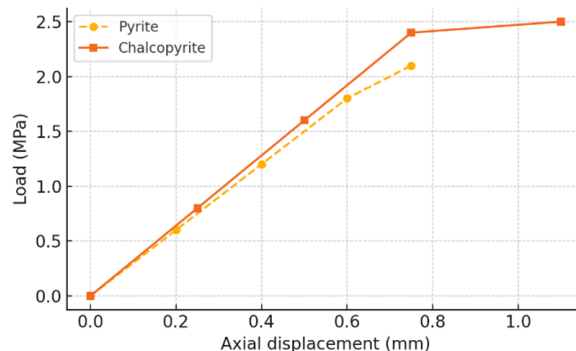


Figure 1. Representative load-displacement curves (Pyrite vs. Chalcocite)

Additionally, Figure 2 presents the boxplot of the tensile strength (σ_t) values differentiated by mineral type. The median σ_t for chalcocite (1.86 MPa) exceeded that of pyrite (1.52 MPa), with a wider range also observed in the latter, reflecting greater internal structural variability in the veinlets.

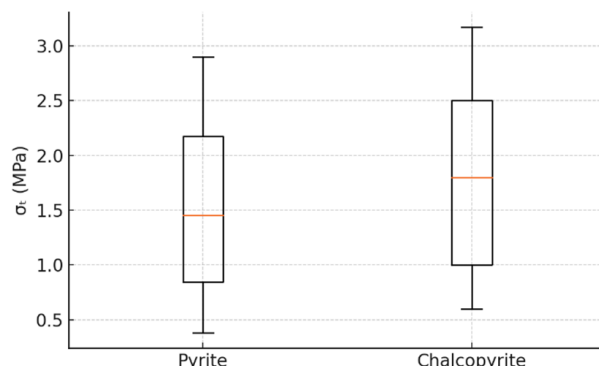


Figure 2. Comparative box plot of tensile strength (σ_t) according to vein type

Finally, Figure 3 shows a positive correlation between the secant modulus (E_s) and the tensile strength (σ_t), showing a joint upward trend. This figure shows that the E_s values increase as σ_t increases, reaching up to 920 MPa in chalcopyrite veinlets and 850 MPa in pyrite veinlets. This validates the hypothesis that stronger mineralized structures also present greater axial stiffness, a behavior consistent with other studies on brittle discontinuities in confined geological environments.

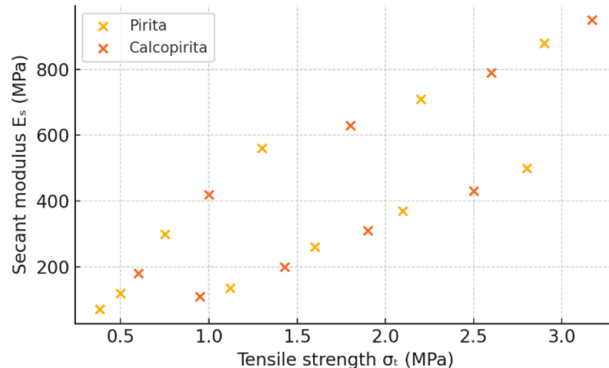


Figure 3. Relationship between E_s and σ_t to analyze tensile behavior

Taken together, these curves suggest that the tensile behavior of veinlets is strongly influenced by their mineralogical composition, effective thickness, and adhesion level at the matrix-mineral interface. The results support the mechanical approach adopted and confirm the applicability of the test for the comparative evaluation of brittle discontinuities.

4 Conclusions

Analysis of direct tensile strength revealed that the chalcopyrite veinlets reached significantly higher values (average σ_t : 1.22 MPa) compared to the pyrite veinlets (average σ_t : 0.58 MPa). This quantitative difference indicates that chalcopyrite exhibits greater internal cohesion and better structural integrity, enabling it to become more resistant to tensile collapse. This finding has direct implications for stability assessment in mineralized zones: structures dominated by chalcopyrite veinlets could be considered more stable under tensional stresses. It is suggested, as a future direction, that these tests be extended to polymetallic veinlets or veinlets with alteration to understand their behavior in more complex scenarios.

The results showed that the average secant modulus in chalcopyrite veinlets was 154.6 MPa, while in pyrite veinlets it was 87.3 MPa. This behavior reflects greater stiffness in chalcopyrite veinlets, which allows less deformation under load and, therefore, greater structural efficiency. In contexts where the integrity of discontinuities must be preserved during excavation or loading cycles, this property represents a crucial differentiating factor. Numerical models in underground mining should incorporate this parameter to define zones with lower support requirements. Future studies could correlate the secant modulus with other mineralogical or microstructural properties.

The load-displacement curves indicated more linear, stiffer, and homogeneous behavior in chalcopyrite veinlets, with an average initial slope of 0.11 kN/mm, compared to 0.06 kN/mm in pyrite. This behavior implies that chalcopyrite transmits axial loads better without concentrations of local stress. In contrast, the dispersion and early nonlinearity in pyrite suggest the existence of microfractures or heterogeneous zones that act as points of anticipated failure. This difference is vital for assessing the mechanical reliability of mineralized bodies in geotechnical structures. It is recommended that these profiles are used to calibrate direct tensile simulations in software such as FLAC3D or UDEC.

The tests indicated that the chalcopyrite veinlets failed predominantly by internal cohesive mode (80%), while the pyrite veinlets showed mixed or interfacial failure of 60%. This difference suggests that chalcopyrite is not only stronger but also has better adhesion to the host rock. The implications of this finding are extended to support design, as areas with pyrite veinlets could act as detachment surfaces and then compromise stability. It is recommended to conduct mineralogical field inspections prior to laboratory tests to identify potentially critical veinlets.

After the tests, the chalcopyrite cleavage surfaces displayed flat facets, metallic luster, and low roughness, while the pyrite veinlets were predominantly rough, oxidized, and debris laden. This difference suggests that pyrite veinlets are more affected by post-depositional physicochemical processes that weaken their cohesion. From an operational perspective, this information is relevant for predicting post-failure behavior, especially in scenarios where fracture planes or induced cracks must be modeled. It is recommended that morphological characterization using microscopy be integrated into future studies to strengthen our understanding of these mechanisms.

Veins with an effective cross-sectional area (A_e) greater than 70 mm³, mainly in chalcopyrite samples, achieved tensile strengths above 1 MPa. This result permits the establishment of a positive correlation between geometry and strength, but it is always dependent on mineralogy. In contrast, in pyrite veinlets, even with similar A_e , strength remained low, thus demonstrating that shape does not compensate for poor mineral quality. This finding emphasizes that mineralogy is the determining factor, while geometry acts as a secondary amplifier. It is recommended that this duality be considered in geotechnical risk assessments at mining faces or ventilation shafts.

It has been quantitatively and experimentally demonstrated that veinlet mineralogy plays a decisive role in their mechanical behavior under direct tensile stresses. Veins composed of chalcopyrite consistently exhibited higher tensile strength of 1.22 MPa, secant modulus of 154.6 MPa, and stiffness values in the load-displacement curve, compared to pyrite veinlets, which recorded average σ_t values of only 0.58 MPa and a secant modulus of 87.3 MPa. This mechanical superiority was also correlated with cohesive failure modes, cleaner rupture surfaces, and a more homogeneous structure, indicating that chalcopyrite not only has better internal strength but also greater adhesion and structural continuity with the rock matrix.

From an applied perspective, these results constituted key technical evidence for evaluating the stability of mineralized zones in underground mining. The ability to identify critical veinlets such as pyrite, based on their tensile behavior and post-failure morphology, allows the optimization of support design and local stability models. The correlation between effective veinlet area and strength was only validated in mineralogically favorable contexts; considering both factors together is also necessary.

These findings are consistent with those reported by Sun et al. [17], who noted that veinlet mineralogy directly influenced the structural response under normal stresses. Likewise, the work of Robbinano et al. [19] on tensile strength in brittle discontinuities supports the methodology used here, especially about the calculation of the secant modulus between 20% and 80% of the maximum load. The morphological classification of rupture surfaces also aligns with the criteria in the study of Aligholi et al. [20] for evaluating fault interfaces.

Unlike previous studies that focused on tensile characterization on bedding planes or natural discontinuities, this work emphasized mineralized veinlets as mechanically active discontinuities and this constitutes a relevant methodological innovation for the geomechanical analysis of orebodies under real-world mining conditions.

Data Availability

The data used to support the findings of this study are available from the corresponding author upon request.

Acknowledgment

This work was supported by the team leading mining projects, whose commitment, dedication, and vision have been fundamental to the success of the initiatives developed. We deeply appreciate their constant support, their innovative approach, and their ability to manage the challenges inherent in the mining industry. Without their hard work and collaboration, this study would not have been possible.

Conflicts of Interest

The authors declare that they have no conflicts of interest.

References

- [1] C. Olmos Maturana, I. Pérez Vargas, G. Uribe Pérez, C. Corvalán Robert, and S. Carstens Soto, “Technological and business lock-in in the Chilean small and medium scale mining,” *Ingeniare. Rev. Chil. Ing.*, vol. 31, p. 28, 2023. <https://doi.org/10.4067/S0718-33052023000100228>
- [2] H. J. Fuentes López, C. C. Ferrucho Parra, and W. A. Martínez González, “Mining and its impact on economic development in Colombia,” *Apuntes Cenes*, vol. 40, no. 71, pp. 189–216, 2021. <https://doi.org/10.19053/01203053.V40.N71.2021.12225>
- [3] Y. Zhang, H. Qi, C. Li, and J. Zhou, “Enhancing safety, sustainability, and economics in mining through innovative pillar design: A state-of-the-art review,” *J. Saf. Sustain.*, vol. 1, no. 1, pp. 53–73, 2024. <https://doi.org/10.1016/J.JSUSUS.2023.11.001>
- [4] F. Pavloudakis, C. Roumpos, and P. M. Spanidis, “Sustainable mining and processing of mineral resources,” *Sustainability*, vol. 16, no. 19, p. 8393, 2024. <https://doi.org/10.3390/SU16198393>
- [5] J. H. C. Barrios, L. M. S. Jusacamayta, K. B. Argumedo, J. C. M. Rojas, W. J. D. Cartagena, R. G. Palomino, and H. D. C. Vilca, “Optimizing time in horizontal mining excavations: 10 formats inspired by value stream mapping principles,” *J. Eur. Syst. Autom.*, vol. 57, no. 2, pp. 517–531, 2024. <https://doi.org/10.18280/JESA.570221>
- [6] P. A. Botero-Santa, S. Xu, A. F. Nieto-Samaniego, and S. A. Alaniz-Álvarez, “Effect of cooling fractures in the formation of normal faults: The example of Santa María del Río, San Luis Potosí, Mexico,” *Bol. Soc. Geol. Mex.*, vol. 72, no. 1, pp. 1–23, 2020. <https://doi.org/10.18268/bsgm2020v72n1a011019>

- [7] L. Qiu, L. Xie, Y. Qin, J. Wang, S. Liu, and J. Qian, “Study on mechanical properties of interbedded rock masses with microcrack based on thermal-mechanical coupling,” *PLoS One*, vol. 19, no. 2, p. e0280486, 2024. <https://doi.org/10.1371/JOURNAL.PONE.0280486>
- [8] M. C. Süner, “The effect of natural fractures on the mechanical behavior of limestone pillars: A synthetic rock mass approach application,” Ph.D. dissertation, West Virginia University, 2021. <https://doi.org/10.33915/etd.8254>
- [9] Y. Li, X. Min, Y. Ke, J. Fei, D. Liu, and C. Tang, “Immobilization potential and immobilization mechanism of arsenic in cemented paste backfill,” *Miner. Eng.*, vol. 138, pp. 101–107, 2019. <https://doi.org/10.1016/J.MINE.2019.04.041>
- [10] M. R. Garza-Román, F. R. Carrillo-Pedroza, N. G. Picazo-Rodríguez, M. J. Soria-Aguilar, I. Almaguer-Guzmán, and J. Chaidez-Félix, “Effects of pretreatment and leaching medium on the extraction efficiency of Au and Ag from a chalcopyrite leaching by-product,” *DYNA*, vol. 88, no. 218, pp. 119–126, 2021. <https://doi.org/10.15446/DYNA.V88N218.90284>
- [11] K. Bär, T. Reinsch, and J. Bott, “The PetroPhysical Property Database (P3) — A global compilation of lab-measured rock properties,” *Earth Syst. Sci. Data*, vol. 12, no. 4, pp. 2485–2515, 2020. <https://doi.org/10.5194/ESSD-12-2485-2020>
- [12] M. L. Pereira, V. Zanon, I. Fernandes, L. Pappalardo, and F. Viveiros, “Hydrothermal alteration and physical and mechanical properties of rocks in a volcanic environment: A review,” *Earth Sci. Rev.*, vol. 252, p. 104754, 2024. <https://doi.org/10.1016/J.EARSCIREV.2024.104754>
- [13] J. A. Vallejos, K. Suzuki, A. Brzovic, and D. M. Ivars, “Application of Synthetic Rock Mass modeling to veined core-size samples,” *Int. J. Rock Mech. Min. Sci.*, vol. 81, pp. 47–61, 2016. <https://doi.org/10.1016/J.IJRMMS.2015.11.003>
- [14] X. Meng, Z. Wu, B. Lan, H. Jiang, Y. Yang, and W. Wang, “Direct tensile damage process of calcite vein shale based on 3D CT reconstruction,” *Energy Sci. Eng.*, vol. 12, no. 3, pp. 913–933, 2024. <https://doi.org/10.1002/ESE3.1663>
- [15] Y. Wu, J. Liu, Z. Wu, J. Liu, Y. Zhao, H. Xu, J. Wei, and W. Zhong, “A universal direct tensile testing method for measuring the tensile strength of rocks,” *China Univ. Min. Technol.*, vol. 34, no. 10, pp. 1443–1451, 2024. <https://doi.org/10.1016/j.ijmst.2024.09.009>
- [16] Y. Liu, G. Zhang, J. Qiao, and X. Tang, “Micromechanical testing and property upscaling of planetary rocks: A critical review,” *China Univ. Min. Technol.*, vol. 34, no. 9, pp. 1217–1241, 2024. <https://doi.org/10.1016/j.ijmst.2024.08.002>
- [17] Z. Sun, P. Li, X. Du, and X. Yang, “Experimental study on the effect of single structural plane on the stability of shallow tunnel surrounding rock,” *Appl. Sci.*, vol. 13, no. 3, p. 1946, 2023. <https://doi.org/10.3390/APP13031946>
- [18] B. Huang, L. Li, Y. Tan, R. Hu, and X. Li, “Investigating the meso-mechanical anisotropy and fracture surface roughness of continental shale,” *J. Geophys. Res. Solid Earth*, vol. 125, no. 8, 2020. <https://doi.org/10.1029/2019JB017828>
- [19] F. Robbiani, K. Liu, Q. B. Zhang, and L. F. Orellana, “Dynamic uniaxial compression testing of veined rocks under high strain rates,” *Int. J. Rock Mech. Min. Sci.*, vol. 153, 2022. <https://doi.org/10.1016/j.ijrmms.2022.105085>
- [20] S. Aligholi, A. R. Torabi, and M. Khandelwal, “Quantifying the cohesive strength of rock materials by roughness analysis using a domain based multifractal framework,” *Int. J. Rock Mech. Min. Sci.*, vol. 170, 2023. <https://doi.org/10.1016/j.ijrmms.2023.105492>